Crystalline Molecular Assemblies of Complexes Showing Eightfold Coordinated Niobium(IV) Dodecahedral Geometry in the Pyridine- Dicarboxylic Acid System

Despoina Andriotou, Sylvain Duval, Christophe Volkringer, Angel Arevalo Lopez, Pardis Simon, Herve Vezin, Thierry Loiseau

Crystalline molecular assemblies of complexes showing eight-fold coordinated niobium(IV) dodecahedral geometry in the pyridine-dicarboxylic acid system

Despoina Andriotou,[a] Sylvain Duval,[a] Christophe Volkringer,[a] Angel M. Arevalo-Lopez,[a] Pardis Simon,[a] Hervé Vezin,[b] and Thierry Loiseau[a,*]

Contribution from
[a]*Unité de Catalyse et Chimie du Solide (UCCS) – UMR CNRS 8181, Université de Lille, Centrale Lille, Université d'Artois, F-59000 Lille, France.*
[b]*Laboratoire de Spectroscopie pour les Interactions, la Réactivité & l'Environnement (LASIRE) – UMR CNRS 8516, Université de Lille, F-59000 Lille, France.*

[*] To whom correspondence should be addressed. E-mail: thierry.loiseau@univ-lille.fr, Phone: (33) 3 20 43 41 22, Fax: (33) 3 20 43 48 95.

To be submitted to Inorg. Chem.
Version May 13, 2022
Revised version July 13, 2022

Table of Content (TOC) Graphic

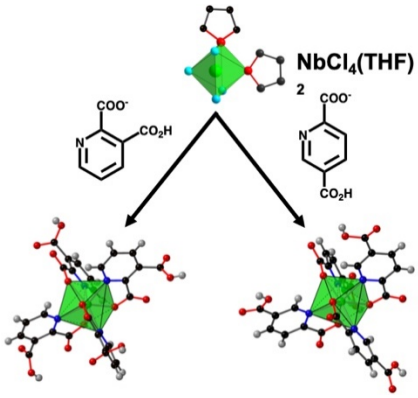

Table of Content (TOC) Synopsis

The monoprotonated 2,3-pyridine-dicarboxylate and 2,5-pyridine-dicarboxylate ligands have been used for the isolation of molecular coordination complexes bearing mononuclear eight-fold coordinated niobium(IV) cations in different crystalline assemblies.

ABSTRACT: The reactivity of the 2,3-pyridine-dicarboxylic (known as quinolinic or H_2qui) acid and 2,5-pyridine-dicarboxylic (known as isocinchomeronic or H_2icc) acid has been investigated as complexing agent toward the niobium(IV) tetrachloride precursor ($NbCl_4 \cdot 2THF$) in different organic solvent mixtures. It resulted in the isolation of four crystalline assemblies of mononuclear coordination complexes **1**-**4** [Nb(HL)$_4$·solvent] where HL is the monoprotonated quinolinate (Hqui) ligand (complexes **1**-**3**) or the monoprotonated isocinchomeronate ligand (complex **4**). For each complex, the discrete niobium(IV) center is eight-fold coordinated to four oxygen atoms from the deprotonated carboxylate arm and four nitrogen atoms from pyridine part of the dicarboxyl ligand with a dodecahedral environment [NbO_4N_4]. The remaining carboxyl arm (either in 3 or 5 position) remained under its protonated form, leading to neutral [Nb(HL)$_4$] moieties for compounds **1**, **2** and **4**, or anionic [Nb(qui)(Hqui)$_3$]$^-$ moiety for compound **3**. The complexes are observed in various molecular arrangements, involving intercalated solvent molecules such as acetonitrile in compound **1** ([Nb(Hqui)$_4$·0.8(CH_3CN)], obtained at room temperature), mixture of acetonitrile and pyridine in compound **2** ([Nb(Hqui)$_4$·0.7CH_3CN·2PYR], obtained via solvothermal reaction at 80°C), mixture of pyridine and triethylamine, in addition with water and chloride species, in compound **3** **(**[Nb(qui)(Hqui)$_3$·Cl·HPYR·HTEA·1.5H_2O], obtained via solvothermal reaction at 80°C), and N,N-dimethylformamide in compound **4** ([Nb(Hicc)$_4$·6DMF], obtained at room temperature). The d^1 configuration expected for the niobium(IV) centers has been analyzed by magnetic measurements, as well as by EPR and XPS. An anti-ferromagnetism transition has been observed at very low temperature for complexes **1** (3.6 K) and **4** (3.3 K), for which the shortest Nb···Nb interatomic lengths occur.

Keywords: niobium(IV), quinolinic acid, isocinchomeronic acid, molecular coordination complex, single-crystal X-Ray diffraction, infrared and EPR spectroscopy, magnetism, XPS.

Introduction

For the last decades, the research of coordination polymers or metal-organic framework (MOF) materials implying tetravalent transition metals has been successfully illustrated by the discovery of promising porous architectures, such as the most well-known families related to the zirconium(IV)-containing compounds of the UiO-66 series[1,2] and its derivatives with hafnium(IV)[3,4] or titanium(IV)-containing compounds (see for instance, MIL-125).[5] The Ti, Zr and Hf metals belong to the same group IV in the periodic table, but other elements such as vanadium(IV) from the adjacent group V can be incorporated into a MOF network (MIL-47), which exhibits a breathing channel system of MIL-53 type.[6] Indeed, the exploration of the periodic table did not show so many other candidates among the high valence metals, except the series of lanthanides (with cerium(IV)[3,7] or actinides[8,9]). Concerning the transition metals of group V, the niobium and tantalum elements have been reported in rare cases of MOF compounds, in which they can be incorporated or used for the construction of three-dimensional porous networks.[10] An unique tantalum(V)-based MOF has been produced by using 2,6-pyridinedicarboxylic acid giving rise to a porous nano-structural solid with high surface area of 1940 $m^2.g^{-1}$. Regarding the parent element niobium(V), it can be inserted in MOF networks via post-synthesis route[11–14] and used as pillar anionic oxyfluorinated brick [$Nb^{V}OF_5^-$] for the formation of open frameworks with narrow pores, devoted to the molecular sieving of small molecules (CO_2, SO_2, etc…).[15–20] In the previous cited works, niobium is commonly utilized under its pentavalent oxidation state, but its reduced form (i.e. +IV, +III states) is much less explored. Nevertheless, Long and co-workers[21] have recently described an original crystalline two-dimensional lattice compound involving the use of a reduced form of starting niobium precursor ($Nb^{III}Cl_3$(DME) reactants) with dihydroxybenzoquinone derivatives linkers. The resulting framework is built up from a honeycomb-like hexagonal layered net, with nodes of niobium centers connected to each other through the dihydroxybenzoquinone species. The determination of the niobium oxidation was quite delicate in this compound, due to the presence of the organic benzoquinone acting as redox trapping linker. The XAS study revealed a Nb(IV) state, whereas magnetic measurements rather assumed a Nb(V) state.

Considering the tetravalent state for niobium, one might expect the formation of a structural variety of networks, compared to the large number of MOF compounds bearing titanium(IV) associated to carboxylate organic linkers, for instance.[22–24] Indeed, the occurrence of niobium(IV) carboxylate coordination complexes is quite limited in literature, whereas the existence of niobium(V) carboxylate are reported in several compounds.[25] The niobium(IV) moieties are observed in molecular mononuclear systems when associated to the oxalate[26], *N*,*N*-diethylcarbamate[27,28] or 2-pyridine-carboxylate (picolinate)[29] ligands (*L*) inducing a [$Nb^{IV}(L)_4$] type entity, or with the ethylenediaminetetraacetate (edta)[30,31] molecule in the compound [Nb^{IV}(edta)(H_2O)$_2$]·2H_2O. There is only one example of a polynuclear oxo-cluster, involving six niobium(IV) atoms and trichloro(or fluoro)-acetate ligands in [$Nb^{IV}_6O_3(O_2CCX_3)_6(OEt)_{12}$] (X = F, Cl).[32] It defines a six-membered ring, in which the niobium centers are linked to each other through μ_3-oxo bridges together with bidentate acetates, alternating with double bridges of oxo groups from ethoxy molecules.

These different compounds revealed that the use of polytopic carboxylate ligands was not so much investigated with niobium(IV). In this contribution, we describe the reactivity of two pyridine-dicarboxylic acids (2,3-pyridine-dicarboxylic acid or quinolinic acid – H_2qui, and 2,5-pyridine-dicarboxylic acid or isocinchomeronic acid – H_2icc) with the niobium(IV) tetrachloride precursor ($NbCl_4 \cdot 2THF$). Four coordination complexes bearing niobium(IV) have been identified at room temperature or mild solvothermal synthesis (at 80°C) in a close cell. Three of them have been obtained with the quinolinic acid, by varying the reaction medium (acetonitrile: compound **1**, [Nb(Hqui)$_4 \cdot 0.8(CH_3CN)$]) with the addition of different organic bases such as pyridine (compound **2**, [Nb(Hqui)$_4 \cdot 0.7CH_3CN \cdot 2$PYR]) and triethylamine (compound **3**, [Nb(qui)(Hqui)$_3 \cdot$Cl$\cdot H$PYR$\cdot H$TEA$\cdot 1.5H_2O$]). A fourth compound (**4**) have been prepared with the isocinchomeronic acid in N,N-dimethylformamide ([Nb(Hicc)$_4 \cdot 6$DMF]). Their single-crystal X-ray diffraction structural arrangement is presented as well as the XPS analysis. As a transition metal with the d^1 configuration, the magnetism measurements and EPR spectra have been collected for all the compounds in order to characterize the niobium(IV) state.

Experimental Section

Reagents. The following reactants were used: niobium tetrachloride tetrahydrofuran (THF) complex ($NbCl_4 \cdot 2THF$, Sigma-Aldrich), 2,3-pyridine-dicarboxylic acid ($C_7H_5NO_4$, known as quinolinic acid, noted H_2qui, 99%, Sigma-Aldrich), 2,5-pyridine-dicarboxylic acid ($C_7H_5NO_4$, known as isocinchomeronic acid, noted H_2icc, 98%, Sigma-Aldrich), acetonitrile (CH_3CN, anhydrous 99.8%, Sigma-Aldrich), pyridine (C_5H_5N, noted PYR, anhydrous 99.8%, Sigma-Aldrich), N,N-dimethylformamide (C_3H_7NO, noted DMF, 99.8%, Sigma-Aldrich) and triethylamine ($C_6H_{15}N$, noted *TEA*, Aldrich, 68%,). The chemical reactants were commercially available, were used without any further purification and manipulated in a glove box under argon to prevent any oxidation of niobium(IV) into niobium(V).

Syntheses

Compound 1 [Nb(Hqui)$_4 \cdot 0.8(CH_3CN)$] : A mixture of 12 mg (0.05 mmol) $NbCl_4 \cdot 2THF$, 15 mg (0.1 mmol) 2,3-pyridine-dicarboxylic acid and 1 mL (19 mmol) acetonitrile was placed in a 2 mL glass tube, sealed with a phenolic cap. Upon the addition, the reaction starts as a precipitate with the formation of brick-like brownish orange crystals, observed after 3 hours at room temperature. After 3 days, compound **1** was analyzed by optical and scanning electron microscope showing elongated parallelepiped-shape crystals of 200-400 μm size. The resulting brownish-orange crystals were then filtered off, washed with chloroform and dried at room temperature in air atmosphere. Crystallization yield was 61.8 $\%_{Nb.}$ (30.9 $\%_{L}$) (Figures S1a and S1c). Compound **1** is stable for few hours under air. Elemental chemical analysis: calculated C: 44.8%, H: 2.7%, N: 8.5%; experimental C: 44.7 %, H: 2.6 %, N: 8.0 %.

Compound 2 [Nb(Hqui)$_4 \cdot 0.7CH_3CN \cdot 2$PYR] : A mixture of 12 mg (0.05 mmol) $NbCl_4 \cdot 2THF$, 16.7 mg (0.1 mmol) 2,3-pyridine-dicarboxylic acid, 1 mL acetonitrile (19 mmol) and 0.5 mL pyridine (6.21 mmol) was placed in a 2 mL glass tube, sealed with a phenolic cap. Octahedrally-facetted brownish-orange crystals have been observed after heating at 80°C for 24 hours in an

oven. The resulting crystalline powder was then filtered off, washed with chloroform and dried at room temperature under argon atmosphere in a glove box. Crystallization yield was 13.9 $\%_{Nb}$ (6.9 $\%_{L}$). Compound **2** was analyzed by scanning electron microscope showing well-shaped octahedrally-facetted crystals of ≈100 µm size (Figures S1a and S1c). Compound **2** is not stable under air. Elemental chemical analysis: calculated C: 50.1%, H: 3.0%, N: 9.9%; experimental C: 48.9 %, H: 2.9 %, N: 8.6 %.

Compound 3 [Nb(qui)(*H*qui)$_3$·Cl·*H*PYR·*H*TEA·1.5H$_2$O]: A mixture of 12 mg (0.05 mmol) $NbCl_4$·2THF, 16.7 mg (0.1 mmol) 2,3-pyridine-dicarboxylic acid, 1 mL acetonitrile, 0.5 mL pyridine (6.21 mmol) and 10 µL TEA (0.07 mmol) was placed in a glass tube, sealed with a phenolic cap and then heated at 80°C for 24 hours in an oven. The resulting black block shaped crystalline powder was then filtered off, washed with chloroform and dried at room temperature under argon atmosphere in a glove box. Crystallization yield was 12.0 $\%_{Nb}$ (6.0 $\%_{L}$). Compound **3** was analyzed by scanning electron microscope showing block like crystals of 30 µm size (Figures S1b and S1d). Compound **3** is not stable under air. In case of 5 acetonitrile molecules (not revealed by single-crystal XRD analysis, elemental chemical analysis is: calculated C: 48.0%, H: 4.0%, N: 10.8%; experimental C: 47.6 %, H: 3.8 %, N: 9.7 %.

Compound 4 [Nb(*H*icc)$_4$·6DMF] : A mixture of 12 mg (0.05 mmol) $NbCl_4$·2THF, 16.7 mg (0.1 mmol) isocinchomeronic acid, 1mL (13 mmol) N,N-dimethylformamide was placed in a glass tube, sealed with a phenolic cap. Upon the addition, the reaction starts as a precipitate with the formation of black octahedral-shaped crystals, observed after 24 hours at room temperature. After 3 days, compound **4** was analyzed by optical and scanning electron microscope showing black octahedral-shaped crystals of 20-30 µm size. The resulting brownish crystalline powder was then filtered off, washed with chloroform and dried at room temperature in air atmosphere. Crystallization yield was 35.2 $\%_{Nb}$ (17.6 $\%_{L}$). Compound **4** was analyzed by scanning electron microscope showing black octahedral-shaped crystals of 20-30 µm size (Figures S1b and S1d). Compound **4** is stable for few hours under air. Elemental chemical analysis: calculated C: 46.2 %, H: 4.8%, N: 11.7%; experimental C: 45.1 %, H: 4.5 %, N: 10.9 %.

Single-crystal X-ray diffraction

Crystals of compounds **1-4** were selected under polarizing optical microscope and glued on a glass fiber for single-crystal X-ray diffraction experiments. X-ray intensity data were collected on a Bruker DUO-APEX2 CCD area-detector diffractometer using Mo-K_α radiation (λ = 0.71073 Å) with an optical fiber as collimator at 100K under nitrogen flux. Several sets of narrow data frames (10s per frame for compounds **1**, **2** and **4**, 25s per frame for compound **3**) were collected with ω scans. The single-crystal XRD intensities were measured on a Bruker DUO-APEX2 diffractometer using Mo-$K\alpha$ radiation (λ = 0.71073 Å). Data reduction was accomplished using SAINT V8.34a.[33] The substantial redundancy in data allowed a semi-empirical absorption correction (SADABS V2014/5)[34] to be applied, on the basis of multiple measurements of equivalent reflections. The structures were solved by direct methods,

developed by successive difference Fourier syntheses, and refined by full-matrix least-squares on all data using SHELX[35] program suites, implemented in the OLEX2[36] interface.
The crystal data are given in Table 1. Supporting information is available in CIF format. CCDC numbers: 2171872 for **1**, 2171873 for **2**, 2171874 for **3** and 2171875 for **4** contain the supplementary crystallographic data for this paper. These data can be obtained free of charge from The Cambridge Crystallographic Data Centre via www.ccdc.cam.ac.uk/data_request/cif.

Table 1. Crystal data and structure refinement for compounds **1 - 4**.

	1	**2**	**3**	**4**
Formula	$C_{29.66}H_{21.31}N_{4.83}NbO_{16}$	$C_{39.4}H_{28.1}N_{6.7}NbO_{16}$	$C_{78}H_{74}Cl_2N_{12}Nb_2O_{35}$	$C_{46}H_{58}N_{10}NbO_{22}$
Formula weight	794.28	944.29	1996.21	1193.69
Temperature/K	103	100	100	100
Crystal type	brownish-orange block	brownish-orange octahedron	brown block	dark blue block
Crystal size/mm	0.41 x 0.27 x 0.17	0.27 x 0.20 x 0.18	0.11 x 0.09 x 0.04	0.2 x 0.1 x 0.1
Crystal system	tetragonal	monoclinic	triclinic	tetragonal
Space group	*P4/ncc*	*C*2/*c*	*P*-1	$I4_1/a$
a/Å	14.5184(11)	19.2258(4)	13.6480(7)	17.3445(8)
b/Å	14.5184(11)	14.0993(3)	13.8277(7)	17.3445(8)
c/Å	14.2771(10)	16.0613(4)	14.5164(7)	18.4014(10)
α/°	90	90	93.994(3)	90
β/°	90	117.0518(9)	100.661(3)	90
γ°	90	90	115.361(2)	90
Volume/Å^3	3009.4(5)	3877.42(15)	2398.4(2)	5535.7(6)
Z, $\rho_{calculated}$/g.cm^{-3}	4, 1.753	4, 1.618	1, 1.382	4, 1.432
μ/mm^{-1}	0.492	0.397	0.381	0.304
Θ range/°	1.98 - 26.44	1.87 - 30.51	1.45 - 26.41	1.61 - 26.36
Limiting indices	$-18 \le h \le 18$ $-18 \le k \le 18$ $-17 \le l \le 17$	$-27 \le h \le 25$ $-20 \le k \le 18$ $-22 \le l \le 20$	$-17 \le h \le 17$ $-16 \le k \le 17$ $-17 \le l \le 18$	$-21 \le h \le 19$ $-21 \le k \le 20$ $-22 \le l \le 22$
Collected reflections	105224	32120	38119	34413
Unique reflections	1561 [R(int) = 0.0368]	5916 [R(int) = 0.0221]	9556 [R(int) = 0.0653]	2835 [R(int) = 0.0333]
Parameters	188	327	584	198
Number of restraints	85	0	18	0
Goodness-of-fit on F^2	1.052	1.083	1.025	1.063
Final R indices [I>2σ(I)]	R1 = 0.0552 wR2 = 0.1558	R1 = 0.0358 wR2 = 0.0950	R1 = 0.0753 wR2 = 0.1933	R1 = 0.0290 wR2 = 0.0722
R indices (all data)	R1 = 0.0704 wR2 = 0.1822	R1 = 0.0384 wR2 = 0.0970	R1 = 0.1136 wR2 = 0.2154	R1 = 0.0338 wR2 = 0.0753
Largest diff. peak and hole/e.Å^{-3}	1.35 and -0.74	0.76 and -0.68	1.25 and -1.57	0.437 and -0.279

Powder X-ray diffraction

X-ray powder diffraction was performed on Bruker D8 Advance diffractometer (LynxEye detector) in a Bragg-Brentano θ-θ mode using Cu-K$_\alpha$ radiation. Each powder pattern was recorded within an angular range of 5-50° in 2θ, with steps of 0.02° and counting time of 0.5 s per step. The compounds **2** and **3**, which have been observed unstable in air, have been put in an airtight specimen holder.

Scanning electron microscopy

The SEM analyses of niobium(IV) coordination complexes **1-4** were performed on a Hitachi-S3400N microscope, equipped with a tungsten filament (acceleration voltage = 15 kV, secondary electron mode, working distance = 5 to 10 mm).

Infrared spectroscopy

Infrared spectrum was measured on Perkin Elmer Spectrum Two™ spectrometer between 4000 and 400 cm^{-1}, equipped with a diamond Attenuated Total Reflectance (ATR) accessory. No ATR correction was applied on the spectrum.

Magnetism

Magnetization measurements were performed in Field Cooled (FC) and Zero Field Cooled (ZFC) procedures with 0.1 T of external magnetic field in a DynaCool 9T PPMS from Quantum Design. Isothermal hysteresis magnetization measurements against magnetic field were collected at selected temperatures in the same apparatus.

EPR spectroscopy.

X-band Continuous-Waver Electron Paramagnetic Resonance (CW-EPR) experiments were carried out at room temperature using a Bruker ELEXSYS E500 spectrometer. CW spectra were collected using 1 G amplitude modulation and 1 mW microwave power.

Echo Field Sweep and 2D-HYSCORE experiments were recorded at X and Q bands with the following pulse scheme: $\pi/2-\tau-\pi/2-t1-\pi-t2-\pi/2-t$ echo and a four-step phase cycling. Pulse lengths were respectively 16 ns and 32 ns for $\pi/2$ and π pulses at X-band whereas this values were set as 8ns and 16ns for Q band measurements. The echo is measured as a function of t_1 and t_2, with t_1 and t_2 being incremented by steps of 16 ns (X band) and 8ns (Q Band) from their initial values. An optimum τ value of 136 ns was used. All the measurements were carried out at 5 K using a CoolEdge cryofree cryostat system.

X-Ray Photoelectron Spectroscopy

X-ray photoelectron spectroscopy (XPS) analysis was performed on a Kratos Axis Ultra DLD spectrometer equipped with a monochromatized Al X-ray source ($h\nu$ = 1486.6 eV) working at 180 W (15 kV, 12 mA).

Prior to analysis the samples were outgassed under primary vacuum (5 Pa) at room temperature for one hour. The XPS analysis chamber was operated under ultrahigh vacuum with a base pressure of 5.10^{-10} Torr. During all analysis the Kratos charge neutralizer system was used. For each sample, binding energy (BE) values were referenced to the adventitious C-C bond component of the C 1s spectra set at 284.8 eV. General survey spectra were acquired with a 160 eV pass energy and C 1s, N 1s, O 1s and Nb 3d core levels spectra with a 20 eV pass energy. A Shirley type background subtraction was applied and spectra were fitted with 70 % Gaussian – 30 % Lorentzian peaks with CasaXPS software.

Results and discussion

Synthesis route

The reactivity of two types of pyridine-based dicarboxylic acids (quinolinic acid or isocinchomeronic acid) with niobium(IV) tetrachloride salt led to the isolation of four distinct crystalline compounds. These reactants are mixed in a glass vial by using either acetonitrile solvent (compounds **1**-**3**) or N,N-dimethyformamide solvent (compound **4**), inside a glove box under inert atmosphere (argon) in order to prevent any oxidation of Nb(IV) to Nb(V). The organic solvents were chosen as both of them solubilized satisfyingly the pyridine-dicarboxylic acid derivated ligands and niobium(IV) precursor. Then, the vials are kept closed until crystallization, whether they are heated (at 80°C for compounds **2** and **3**, for one day) or not (room temperature crystallization for compounds **1** and **4**, for three days).

In a first attempt, the strategy was to study the connection arrangement of the ditopic 2,3-pyridine-dicarboxylate ligand around the niobium(IV) center. It was observed (structure description section) that only one carboxylate arm and neighboring nitrogen atom of the pyridine ring was involved in the coordination sphere of the 4*d* metal (compound **1**).

Since the second carboxylate arm of the quinolinate ligand remains under its protonated state in compound **1**, we investigated the influence of the addition of an organic base in order to tentatively obtain the di-anionic form of the ditopic carboxylate ligand ($^{-}O_2C\text{-}C_5H_5N\text{-}CO_2^{-}$), with the aim to further condense a second niobium(IV) center with this type of linker. For these attempts, we used pyridine (pK_a = 5.23) as additional solvent with acetonitrile (compound **2**) and a mixture of pyridine / triethylamine (pK_a = 10.75) together with acetonitrile (compound **3**). It is interesting to notice that the crystalline phases of compounds **2** and **3** appeared only after a solvothermal treatment of the starting solution after heating at 80°C, for 24 hours, but with lower reaction yields (in the range 12.-14 %, based on Nb) instead of 62-35% (based on Nb) for the compounds **1** and **4**, synthesized at room temperature. Although the addition of organic bases (pyridine, triethylamine) in the reaction medium, a similar connection mode of the quinolinate ligand with the niobium(IV) center was found together with a unreacted free carboxylic acid function.

In a last reaction, we study the reactivity of the parent pyridine-dicarboxylic acid, with the two carboxylate functionalities in 2,5 position (isocinchomeronic acid) instead of 2,3 (quinolinic acid), assuming that opposite carboxylate groups may favor the connection of two different niobium(IV) centers (mimicking the 1,4-benzene dicarboxylate or terephthalate configuration, for instance), in order to generate infinite networks. When the isocinchomeronic acid was used, we were able to isolate an analogous complex with niobium(IV), which crystallized in N,N-dimethylformamide solvent (compound **4**), since our attempts for the synthesis route with the acetonitrile solvent were found unsuccessful.

After synthesis no by-product was observed for the four compounds **1**-**4**, and the remaining content of the non-crystallized niobium of pyridinedicarboxylic acid species remained in the supernatant solution. After long exposure to air for compounds **2** and **3**, an amorphous powder is obtained without any trace of the original crystalline complexes. Some attempts were made to add small amounts of water to the chemical system in order to promote a controlled hydrolysis reaction toward niobium(IV) species, but were unsuccessful due to the systematic formation of crystalline NbO_2.

Structure Description

From the structural point of view, all the atomic arrangement of compounds **1**-**4** are based on the same molecular assemblies containing one niobium(IV) center eight-fold coordinated by four bidentate pyridine-based dicarboxylate (2,3-pyridine-dicarboxylate (**1**-**3**), or 2,5-pyridine-dicarboxylate (**4**)) ligands through the carboxyl O and pyridyl N atoms, associated with different extra solvents molecules. The geometry around the niobium(IV) atoms defines a triangulated dodecahedral environment (D_{2d} symmetry; only the single term dodecahedron only will be used in the following text) as expected for eight-fold coordination system of $\{MA_4B_4\}$ unit for d^1 transition cations (Orgel concept[37]). This series of four niobium-centered complexes are closely related to that observed in the niobium(IV) 2-pyridinedicarboxylate (known as picolinate = pic) moiety $[Nb(pic)_4{\cdot}2EtOH]$, previously described by Ooi et al., in 1996.[29]

Crystal structure of compound $Nb(Hqui)_4{\cdot}0.8CH_3CN$ **(1)** possesses one crystallographically unique niobium atom (Nb1), sitting on the special position 4*b* (axis -4) and involved in a mononuclear complex with one crystallographical type of quinolinate (2,3-pyridine-dicarboxylate) ligands, located in general position 16*g*. The niobium center (Nb1) is coordinated by the nitrogen heteroatom (N1) of the pyridine ring and one oxygen atom (O1) from the carboxylate group in position 2, from four quinolinate ligands (Figure 1), leading to the environment $\{NbO_4N_4\}$. The corresponding bond lengths are 2.278(4) Å for Nb1-N1 (4x) and 2.085(3) Å for Nb1-O1 (4x). The dihedral angle between the two interpenetrating planes defined by the O···N···N···O sequence of connecting atoms to the central niobium cation is 90°, revealing the ideal D_{2d} dodecahedral geometry for the $\{NbO_4N_4\}$ unit.[38,39] If the D_{4d} square antiprism geometry is considered, the dihedral angle value will be 77.4° instead. The interatomic Nb-O and Nb-N bond distances are in the range of those encountered in the niobium(IV) complex obtained with a parent pyridine-based monocarboxylate ligand such as the picolinic acid (2-pyridinecarboxylic acid), for which the Nb-O lengths varied from 2.092(2) up to 2.108(1) Å, and Nb-N lengths varied from 2.295(2) up to 2.310(2)(1) Å, from single-crystal XRD data collected at room temperature.[29] The remaining free C1-O2 bond of the monodentate carboxylate group exhibits a length of 1.224(5) Å, revealing its non-protonated state. A part of the pyridine ring was found on two close positions, with a statistical disorder of 56/44 for the C3 → C7 atoms and the O atoms of the second carboxylate arm. For the latter, the bond C-O distances are slightly contrasted with a shorter one (C7B-O5 = 1.233(10) Å) and longer ones (C7B-O6 = 1.268(9) Å, C7A-O4 = 1.271(12) Å and C7A-O3 = 1.274(9)), indicated a typical protonated state.

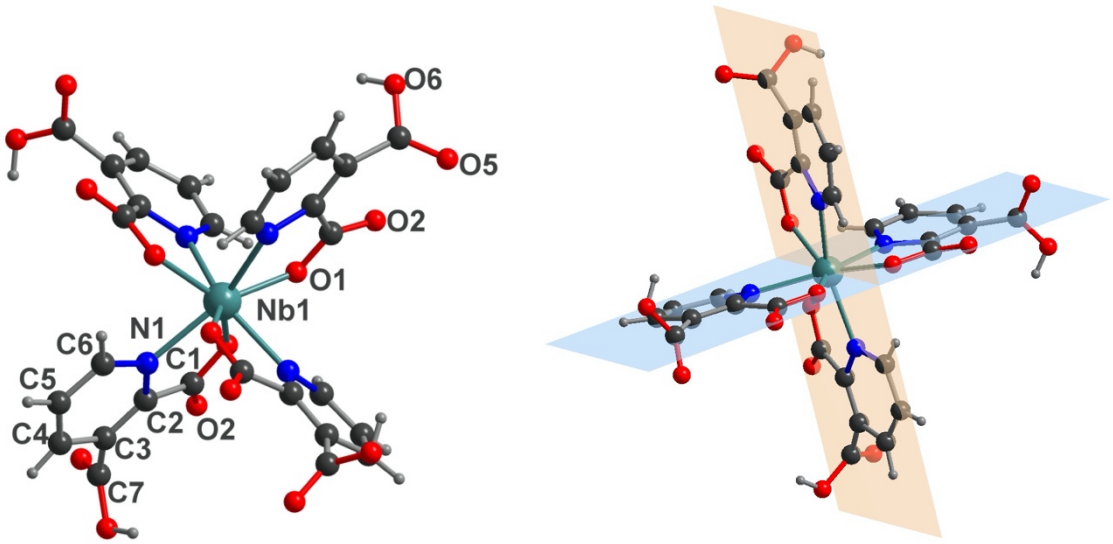

Figure 1. (left) Ball and stick representation of the mononuclear niobium(IV)-centered coordination complex of Nb(*H*qui)$_4$·0.8CH$_3$CN (**1**). Only atom labels of one crystallographically independent quinolinate ligand are shown. (right) view of the two interpenetrating perpendicular planes constructed from the O···N···N···O sequence of connecting atoms to the central niobium cation, with a dihedral angle of 90°. For clarity, the statistical disorder related to the C3, C4, C5, C6, C7, O5 and O6 atoms are not shown. Green circle: Nb; blue: N, red: O; dark grey: C, light grey: H.

The monoprotonated quinolinate linker which is tetra-coordinated to one niobium(IV) center, ensures the electroneutrality of the complex. The supramolecular assembly is based on the stacking of the [Nb(*H*qui)$_4$] species along the *c* axis, with a rotation of around 45° of the pyridine ring fragments between two adjacent niobium centers. It results in the formation of four-pointed star-like channels, in which free acetonitrile solvent resides (Figure 2). This acetonitrile molecule is not well positioned as it seems to be disordered along its own linear axes, running parallel to the *c* axis. Thus, finally $C_{acetonitrile}$ and $N_{acetonitrile}$ occupancies were refined to the value close to 0.8 and 0.4, respectively, corresponding to a crystallographical ratio of 0.8CH$_3$CN for one [Nb(*H*qui)$_4$] species. During the refinement calculations, the protons of methyl group of acetonitrile could not be located due to their free rotation around the linear C-C-N axis related to the tetragonal *c* axis. Within a layer in the (*a*,*b*) plane, each quinolinate molecule interacts to each other, via one terminal carboxylic acid arm pointing perpendicularly toward a neighboring pyridine ring fragment of a second ligand. The remaining free carboxylic acid functions are arranged around the acetonitrile solvent, with C-O···N distances of 2.75(4) Å.

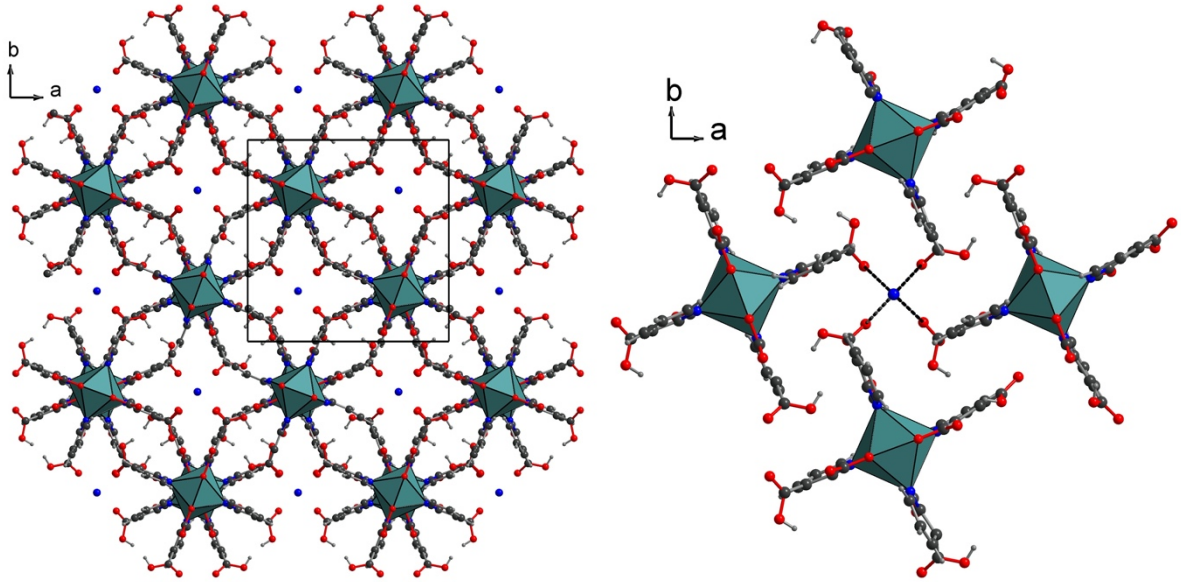

Figure 2. (left) polyhedral view of the packing structure of the neutral [Nb(*H*qui)$_4$] complex arranged around the acetonitrile solvent in compound **1**, along the c axis. (right) detailed view of the arrangement of [Nb(*H*qui)$_4$] moieties in the (*a*,*b*) plane, showing the shortest interactions of the free non-bonded carboxylic acid functions of the quinolinate ligands with acetonitrile. Linear acetonitrile molecules are located along the [001] direction, and only its nitrogen atom (blue circles) are shown. Green polyhedron: Nb; blue circle: N, red: O; dark grey: C, light grey: H.

The structure of compound Nb(*H*qui)$_4$·0.7CH_3CN·2PYR (**2**) exhibits a similar eight-fold coordination sphere around the niobium(IV) atom, as found in complex (**1**) (Figure 1). The niobium cation is surrounded by two types of crystallographically independent quinolinate ligands, through four pyridyl nitrogen and four carboxyl oxygen atoms (in position 2), with Nb-O and Nb-N bonding lengths of 2.090(1)-2.104(1) Å, and 2.286(1)-2.287(1) Å, respectively. These Nb-O and Nb-N bond ranges were similar to those found in compound **1** and related Nb(IV)-picolinate complex.[29] The resulting [NbO_4N_4] polyhedron describes a distorted dodecahedral geometry as defined by the dihedral angle of 87.49(4)° between the two planes from obtained through the sequence of O···N···N···O atoms from the two sets of nearly perpendicular bidentate quinolinate molecules (Figure 3). This angle value is in agreement with a dodecahedral environment around the niobium center[39], even if it is slightly shifted from the ideal case of 90°. The remaining C-O bond is not protonated, with short C7-O3 and C14-O4 distances of 1.220(2) and 1.217(2) Å, respectively.

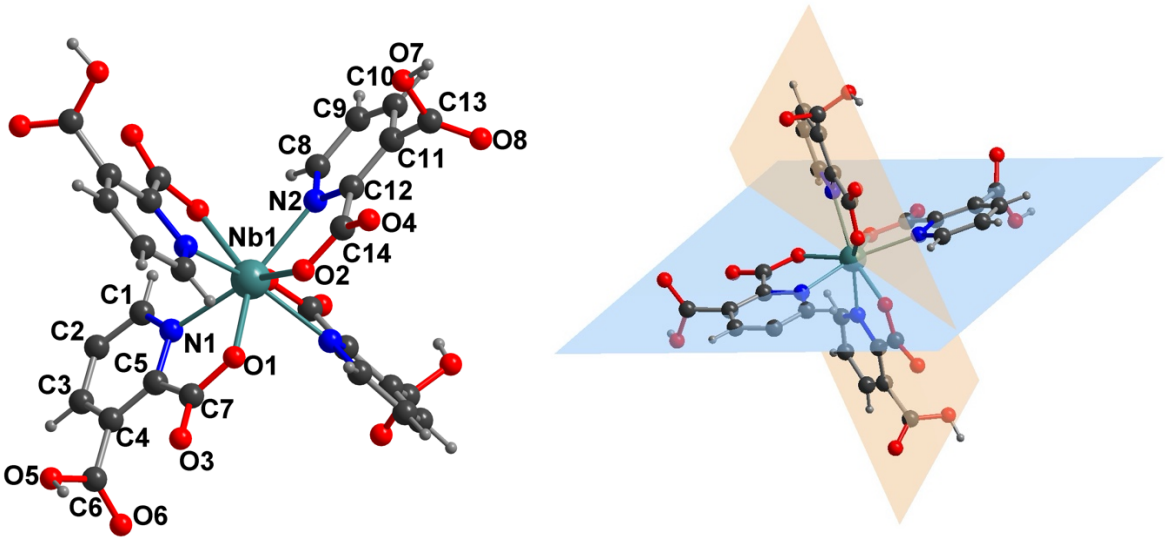

Figure 3. (left) Ball and stick representation of the mononuclear niobium(IV)-centered coordination complex of Nb(*H*qui)$_4$·0.7CH$_3$CN·2PYR (**2**). Only atom labels of two crystallographically independent quinolinate ligand are shown. (right) view of the two interpenetrating perpendicular planes constructed from the O···N···N···O sequence of connecting atoms to the central niobium cation, with a dihedral angle of 87.49(4)°. Green circle: Nb; blue: N, red: O; dark grey: C, light grey: H.

The second carboxylate arm in position 3 is under its protonated form with the two specific contrasted C=O and C-OH bond lengths of 1.211(3)-1.229(2), and 1.276(3)-1.300(3) Å. The crystal packing is constructed from the molecular assembly of neutral Nb(*H*qui)$_4$ entities, which are arranged around pyridine and acetonitrile solvents species, trapped within triangular-shaped pseudo-channels along the [-101] direction (Figure 4). These molecules were found disordered on two positions: there exists an occupancy of 35/65 for pyridine, related to a multiplicity twice related to the niobium center. For acetonitrile, the carbon atoms are also disordered on two positions, with the same occupancy 35/65, around the nitrogen atom, which has a occupancy factor refined to 70%. The interactions of these intercalated pyridine/acetonitrile species with the Nb(*H*qui)$_4$ entities, are rather weak, with interatomic distances greater than 3.2 Å regarding the C-OH bondings of the monoprotonated quinolinate ligands. Thus, the organization of the Nb(*H*qui)$_4$ complexes differs from that observed in compound **1**, through the structuring role of the couple pyridine/acetonitrile in compound **2**, compared to only acetonitrile occurs in compound **1**. One notices preferential strong hydrogen interactions between the terminal carboxylic acid functions (through C-O7H···O5 = 1.660(2) Å) of two adjacent Nb(*H*qui)$_4$ entities, generating chains along the [101] direction (Figure 4).

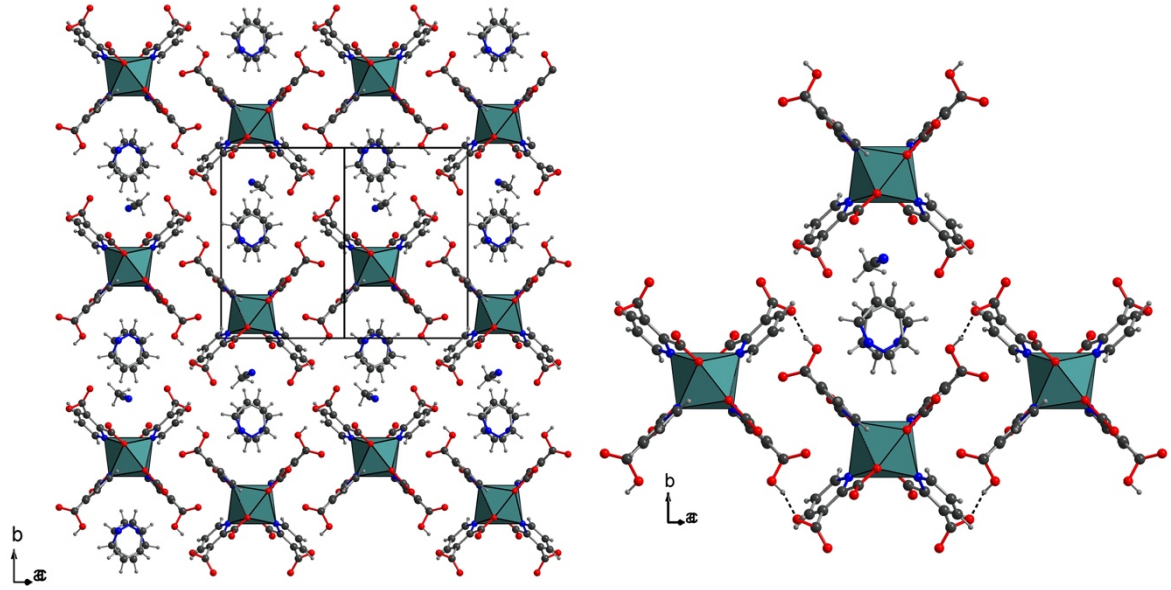

Figure 4. (left) polyhedral view of the packing structure of the neutral [Nb(*H*qui)$_4$] complex arranged around the acetonitrile and pyridine solvent in compound **2**, along the [-101] direction. (right) detailed view of the arrangement of [Nb(*H*qui)$_4$] moieties, showing the shortest interactions of the free non-bonded carboxylic acid functions of the quinolinate ligands to each other along the [101] direction (dotted lines: hydrogen bondings). Disorder of pyridine and acetonitrile solvents are not shown for clarity. Green polyhedron: Nb; blue circle: N, red: O; dark grey: C, light grey: H.

The crystal structure of compound of Nb(qui)(*H*qui)$_3$·Cl·*H*PYR·*H*TEA·1.5H$_2$O (**3**) consists of one niobium(IV) metal center, bound to four distinct crystallographically independent quinolinate ligands (Figure 5). As observed for the other complexes, the niobium atom is eight-fold coordinated to four pyridyl nitrogen atoms (Nb-N = 2.283(5)-2.296(4) Å) and four carboxyl oxygen (Nb-O = 2.084(3)-2.097(4) Å), which are comparable with the Nb-O and Nb-N bondings range encountered for the tetravalent oxidation state of Nb (see compounds **1**-**2**). The coordination sphere around the niobium(IV) cation defines a dodecahedral polyhedron, with dihedral angles between the planes formed by two sets of O···N···N···O atoms sequence from quinolinate linkers, of 89.3(1)° (Figure 5). This value reveals a very weak distortion to the ideal geometry.[39] As for compounds **1**-**2**, the second C-O bonding from the monodentate carboxylate arm is terminal with relatively short C-O bond lengths (C-O = 1.217(6)-1.221(9) Å). For the other carboxylate arm in position, the situation differs, since we observe the protonation for three of the four connecting quinolinate ligands. The expected long C-OH and short C=O bond distances are found with the values of 1.306(10-1.319(7) Å and 1.177(11)-1.205(7) Å, respectively. The fourth quinolinate molecule exhibits the two C5-O bondings from carboxylate arm in position 3, with the values of C5-O3 and C5-O4 of 1.253(6) and 1.258(7) Å, respectively, and indicating its non-protonated state.

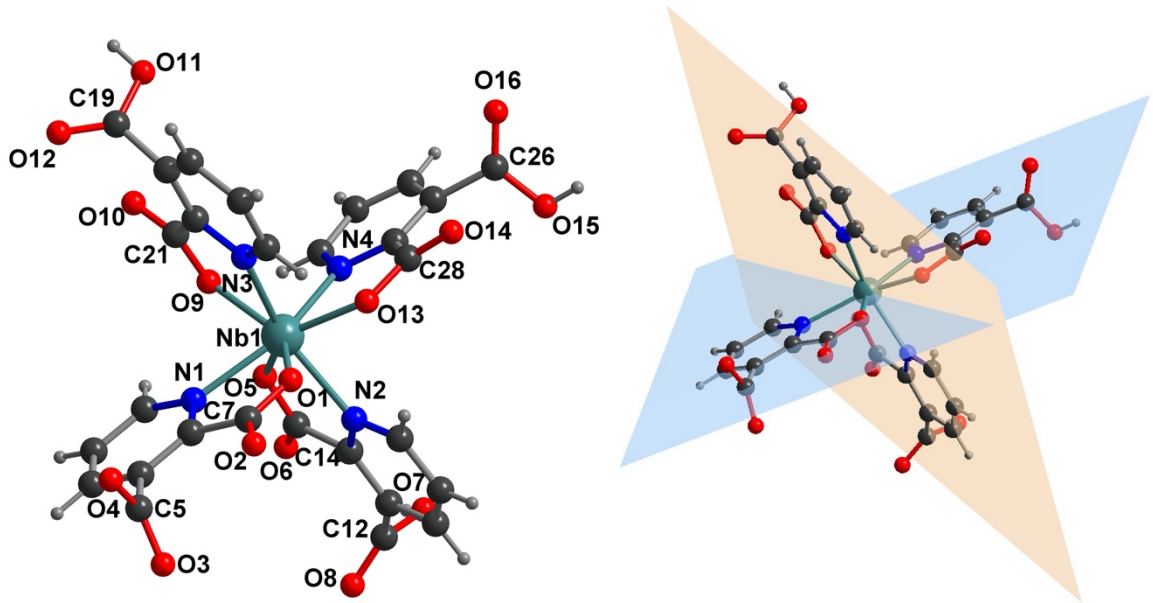

Figure 5. (left) Ball and stick representation of the mononuclear niobium(IV)-centered coordination complex of Nb(qui)(*H*qui)$_3$·Cl·*H*PYR·*H*TEA·1.5H$_2$O (**3**). Atom labels of four crystallographically independent quinolinate ligands are shown, except those of C atoms from pyridine groups, for clarity. (right) view of the two interpenetrating perpendicular planes constructed from the O···N···N···O sequence of connecting atoms to the central niobium cation, with a dihedral angle of 89.3(1)°. Green circle: Nb; blue: N, red: O; dark grey: C, light grey: H.

The occurrence of unprotonated quinolinate ligands attached to niobium atoms results in a negatively charged [Nb(qui)(*H*qui)$_3$]$^-$ entity, which is surrounded by distinct species such as triethylamine, pyridine, isolated chloride anions and water molecules (the latter coming from undried triethylamine precursor) (Figure 6). The pyridine and triethylamine molecules were observed under their protonated form, which thus bring two positive charges, and compensated by the two negative charges from chloride and [Nb(qui)(*H*qui)$_3$]$^-$ anions, ensuring the electroneutrality of the crystalline structure. But, the structure resolution did not allow for identifying properly all the species within the crystal packing of compound **3**. SQUEZZE procedure was used to remove a calculated electronic density of 112 electrons on a void volume of 429 Å^3. These electrons could be assigned to five unlocated acetonitrile molecules. We therefore tentatively propose a schematic view of the different interactions between the intercalated species. Indeed, preferential hydrogen bonds occur between the [Nb(qui)(*H*qui)$_3$]$^-$ entities themselves, through the oxygen atoms from deprotonated carboxylate and carboxylic acid group (O7-H···O3 = 2.075(6) Å and O11-H···O4 = 1.713(5) Å), resulting in the chain-like system, running along the [111] direction (Figure 6). The protonated triethylamine molecule is hydrogen bonded via its central ammonium group to oxygen from deprotonated carboxylate arm, with N5-H···O3 = 1.875(5) Å. The free pyridinium anions preferentially interact through the non-bonded oxygen atom O2, from the carboxylate arm in position 2, belonging to the deprotonated quinolinate ligand (N6-H···O2 = 2.341(7) Å). The water molecule (OW17) is hydrogen bonded to the carboxylic acid function of one quinolinate ligand (O15-H···OW17 = 2.027(7) Å). Other species (Cl, H$_2$O) are weakly interacting with the [Nb(qui)(*H*qui)$_3$]$^-$ units with bond distances greater than 2.8 Å.

Both compounds **2** and **3**, obtained in the presence of additional organic base, revealed that the similar connection mode of the quinolinate ligands with niobium(IV), leaving the second carboxylic acid arm under its protonated form.

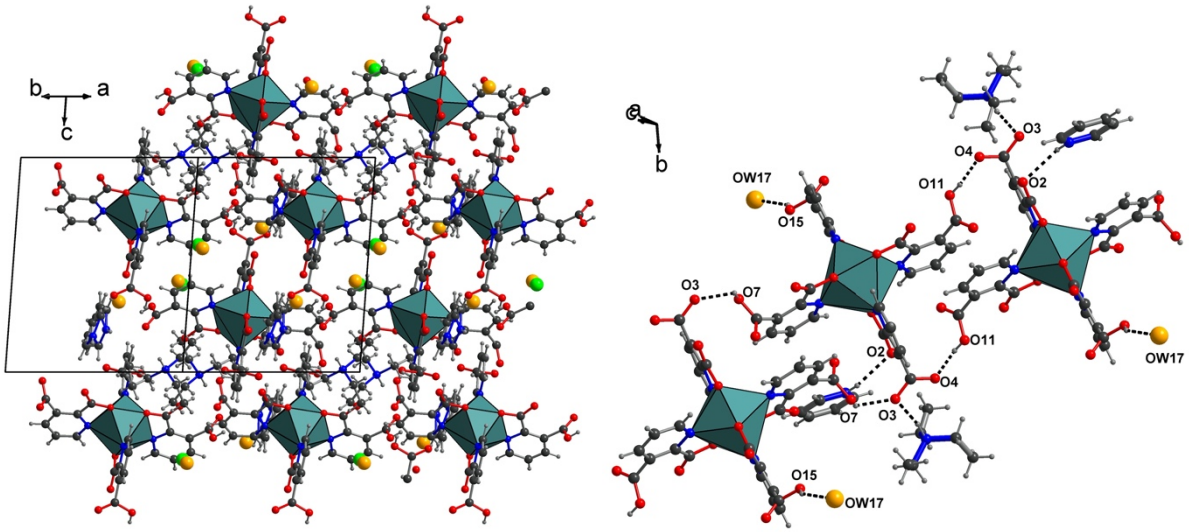

Figure 6. (left) polyhedral representation of the structure of compound Nb(qui)(*H*qui)$_3$·Cl·*H*PYR·*H*TEA·1.5H$_2$O (**3**) along the [110] direction. (right) detailed view of the hydrogen bond interactions between [Nb(qui)(*H*qui)$_3$] entities and with protonated pyridine and triethylamine, and water molecules, along the [111] direction (dotted lines: hydrogen bondings). Pyridine and one methyl group of triethylamine molecules were found to be disordered on two equivalent positions, and are not shown for clarity. Green circle: Nb; blue: N, red: O; dark grey: C, light grey: H; light green: Cl; orange: free water.

The crystal structure (Nb(H*icc*)$_4$·6DMF) (**4**) is built up from one crystallographically unique niobium(IV) atom (Nb1), sitting on the special position 4*b* (axis -4) and linked through pyridinato nitrogen atoms and carboxyl oxygen atoms in position 2 of one crystallographical type of isocinchomeronate (2,5-pyridine-dicarboxylate) ligand, located in general position 16*f* (Figure 7). The four isocinchomeronate linkers adopt a bidentate connection mode with the niobium(IV) center with Nb1-O1 bond distance of 2.1082(11) Å (x4) and Nb1-N1 bond distance of 2.266(2) Å (4x). As for compounds **1-3**, it was observed an ideal dodecahedral geometry for the [NbO$_4$N$_4$] unit, since the dihedral angle between the two interpenetrating planes defined by the O···N···N···O sequence is 90°.[39] The Nb-O and Nb-N bond lengths are in the same range as found in the other compounds **1-3**, for an eight-fold coordinated niobium atom at the tetravalent oxidation state. The second carboxyl oxygen atom of the monodentate carboxylate arm is free, with a rather short C1=O2 distance of 1.224(2) Å, reflecting its expected non-protonated state. The second carboxylic acid function in position 5 is observed as its protonated state, with two typical distinct C7-O4H and C7=O3 bond distances of 1.319(3) Å and 1.205(2) Å, respectively. The molecular assembly of the neutral [Nb(H*icc*)$_4$] moieties are arranged along a square net in the *ab* plane, with intercalated DMF solvent molecules (Figure 8). Two types of DMF species are observed in the crystal packing with different multiplicities: one (noted A in figure 8) strongly interacts with the free carboxylic acid proton of the isocinchomeronate ligand (CO-H···O$_{DMF(A)}$ = 1.728(2) Å), with the same molar ratio (1 *H*icc / 1 DMF$_{(A)}$). The second DMF molecule (noted B in figure 8) has a half multiplicity and

is inserted in pseudo-channel defines by the packing of the [Nb(H*icc*)$_4$···4DMF$_{(A)}$] entities, with weaker interactions (ex: O5$_{DMF(B)}$···O2$_{icc}$ > 3.687(4) Å). The latter is found disordered on two equivalent positions for the carbonyl oxygen and one methyl group.

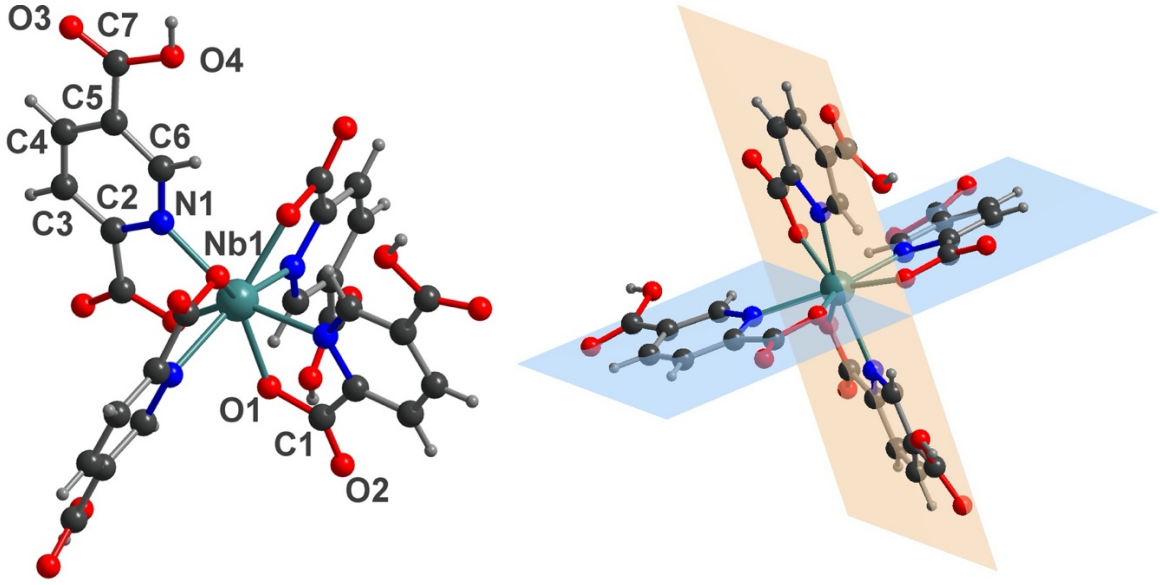

Figure 7. (left) ball and stick representation of the complex Nb(H*icc*)$_4$·6DMF (**4**) showing the eight-fold coordinated niobium(IV) center. Only atom labels of one crystallographically independent isocinchomeronate ligand are indicated. (right) view of the two interpenetrating perpendicular planes constructed from the O···N···N···O sequence of connecting atoms to the central niobium cation, with a dihedral angle of 90°. Green circle: Nb; blue: N, red: O; dark grey: C, light grey: H.

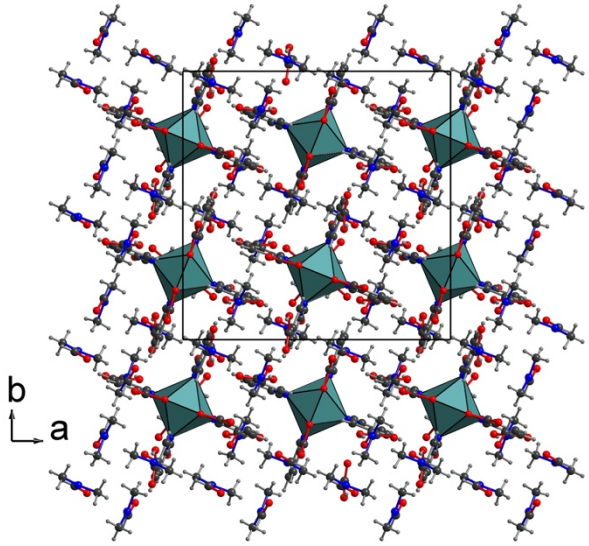

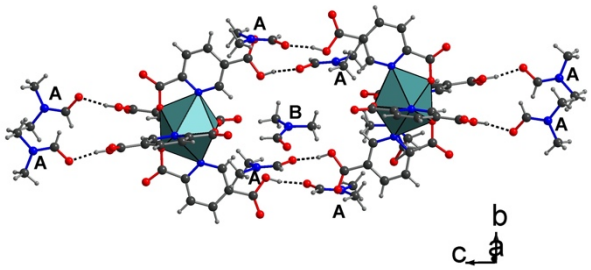

Figure 8. (top) polyhedral view of the packing arrangement of the [Nb(H*icc*)$_4$] moieties intercalated by DMF solvent molecules, in compound **4**, along the *c* axis. (bottom) detailed representation of the two distinct types of DMF solvent molecules: DMF molecules type A are strongly hydrogen-bonded linked to the proton from free carboxylic acid function of isocinchomeronate ligand, forming the entity [Nb(H*icc*)$_4$···4DMF$_{(A)}$]; DMF molecules type B exhibit a disorder for the carbonyl/C-H groups as well as disorder methyl proton. For clarity, only disorder is not shown for this DMF species. Green polyhedron: Nb; blue circle: N, red: O; dark grey: C, light grey: H., dotted line: hydrogen bond between isocinchomeronate ligand and DMF$_{(A)}$ molecules.

Magnetism

Due to the 4d^1 electronic configuration for niobium(IV), we investigated the magnetic behavior of the series of the four molecular compounds **1-4**. Indeed, the magnetic characterization has been rarely reported in literature for such eight-fold coordinated niobium(IV) centers with well-defined geometrical environment (Table 2). The magnetic susceptibility $\chi(T)$ has been measured as a function of the temperature in the range 2-300 K (Figures 9 and S4a-b). The thermal dependence has been fitted classically from the Curie-Weiss law $\chi(T) = C/(T-\theta)$, where T is the temperature, C is the Curie constant and θ is the Weiss constant.

The effective magnetic moment has been extracted from the slope of the linear plot of $\chi^{-1}(T)$ versus T in the range 15-150 K for complex **1**, 50-200 K for complex **2**, 75-200 K for complex **3** and 50-150 K for complex **4**. The experimental effective magnetic moment values, μ_{eff} for the complexes **1-4** were 1.61, 1.50, 1.47 and 1.58 μ_B (Bohr Magnetons), respectively (Figures 9 and S4a-b). These values are ranging around the theoretical one (μ_{eff} = 1.73 μ_B), which correspond to a spin-only system, expected for a single unpaired electron with a d^1 electronic configuration, as it occurs with niobium(IV).[40]

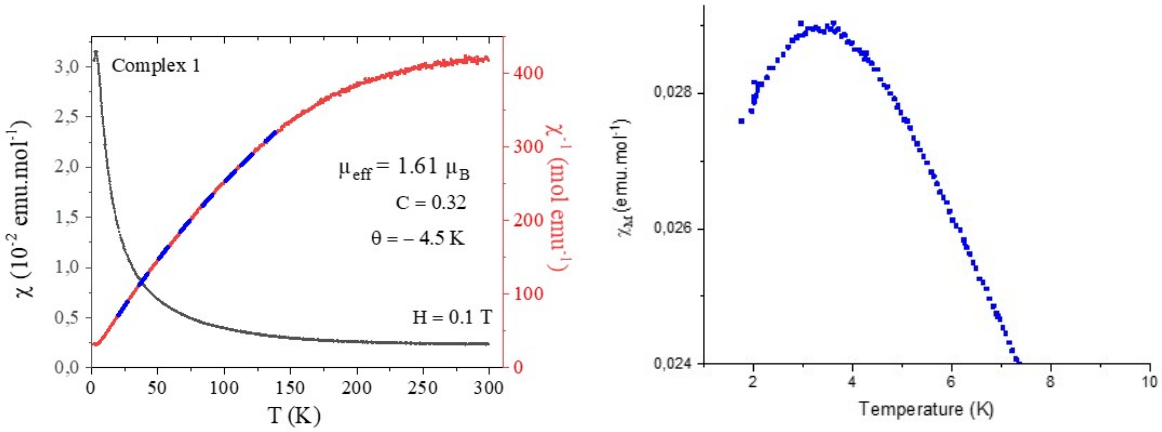

Figure 9. Magnetic susceptibility (χ, ordinate scale in the left, black circles), inverse susceptibility (χ^{-1}, ordinate scale in the right, red circles) curves as a function of temperature for the powdered complexes **1** and linear plot range (dashed blue line) for the estimation of the experimental $\mu eff = 1.61\ \mu_B$ (left). Zoom at the range 2-10 K highlights the transition observed at 3.6 K (right).

Table 2. magnetic moments of eight-fold coordinated niobium(IV) centers in complexes with O and/or N-donor ligand at room temperature.

Compound	Coordination environnent	Geometry	Effective magnetic moment μ_B	Reference
complex **1**	$[NbO_4N_4]$	dodecahedron	1.61	our work
complex **2**	$[NbO_4N_4]$	dodecahedron	1.50	our work
complex **3**	$[NbO_4N_4]$	dodecahedron	1.47*	our work
complex **4**	$[NbO_4N_4]$	dodecahedron	1.58	our work
$Nb(pyc)_4 \cdot 2EtOH$[a]	$[NbO_4N_4]$	dodecahedron	1.44	29
$Nb(O_2CNEt_2)_4$	$[NbO_8]$	dodecahedron	1.55	27
$Nb(acac)_4$[b]	$[NbO_8]$	not reported	1.47	41
$Nb(hfacac)_4$[c]	$[NbO_8]$	square antiprism	1.54	28
$(Pc_2Nb) \cdot ClNP$[d]	$[NbN_8]$	square antiprism	1.69	42

[a]pyc= 2-pyridinecarboxylate ; [b]acetylacetonate ; [c]hexafluoroacetylacetonate ; [d]Pc = phtalocyanine, ClNP = 1-chloronaphthalene.

*this μeff value has been estimated from the chemical formula obtained by single-crystal XRD analysis, without taking into account the non-revealed intercalated molecular species due to the use of SQUEEZE procedure. If five acetonitrile molecules are present in the structure as suggested the number of remaining electrons, it is estimated a value of $\mu eff = 1.52\ \mu_B$.

For two of the complexes (**1** and **4**), it is observed a curvature change a very low temperature on the $\chi(T)$ versus T plot, with T = 3.6 and 3.3 K, respectively (Figure 9 and S4b), and typically related to an antiferromagnetic transition. However, this magnetic susceptibility variation was not visible for the two other complexes **2** and **3**. This magnetic behavior might be correlated to the different supramolecular Nb···Nb distances in each complex. Regarding the shortest distances within a regular or distorted square net of niobium(IV) nodes, we noticed two interatomic length values lower than 10 Å for complexes **1** and **4** and two others greater than 10 Å for complexes **2** and **3** (Table 3). It results that a Nb···Nb distance value greater than 10 Å does not give rise to such antiferromagnetic transition, whereas it exists at lower Nb···Nb distance, with a transition temperature increase inversely to the interatomic length. This behavior is supported also by magnetization experiments, where magnetization (M) is plotted against the magnetic field (H) (Figures S4c). For complexes **1** and **4**, where interatomic niobium atoms see each other, magnetization is harder to achieve and needs a higher magnetic field value. Whereas, for complexes **2** and **3**, magnetization is easier and with lower values of magnetic field.

Table 3. List of the shortest interatomic Nb···Nb distances and antiferromagnetic transition temperature in complexes **1**-**4**.

	shortest Nb···Nb distances (Å)	transition temperature (K)
Complex **1**	7.1385(5)	3.6
Complex **2**	10.1153(16)	none
Complex **3**	13.6479(14)	none
Complex **4**	9.8169(4)	3.3

EPR spectroscopy

In the series of Nb(IV)-containing complexes (**1-4**), the electronic configuration of Nb(IV) is [Kr] $5s^1$ leaving niobium with an unpaired electron and permits further analysis by Electron Paramagnetic Resonance (EPR).

For the three compounds, from the first derivative EPR spectra display in Figure 10, show an EPR signal with a g factor of 1.970(1), 1.968(2) and 1.965(3), which verifies the *d* character of electron, even if no hyperfine structure of the nuclear spin I=9/2 of niobium are observed. Such a result indicates that the electron is no fully localized at room temperature.

Thus, we have performed pulsed EPR experiments a low temperature (5K) using pulse scheme excitation and detection using 2 pulses Hahn echo sequence as a function of field sweep. Such an experiment reveals the overlap of two signals respectively related to Nb(IV) and oxygen dangling bond (Figure S5a).

The signal observed is isotropic with 9 lines observed with an hyperfine coupling of 205 G resulting in 70 % of fraction of the electron in niobium *d* orbitals. We can also observe the hyperfine coupling of niobium(IV) (Figure 11), values close to the ones found in literature.[13]

The intense absorption peak, corresponds to the signal of an oxo group, verifying the existence of a Nb-O bond, in which the electron is delocalized with an equilibrium between $Nb^{\cdot}$-O and Nb-$O^{\cdot}$. By performing Q-band experiments, we can observe a weak anisotropy of the g factor indicating that the symmetry is higher (Figure S5b). On the other side, we can assume that there is a weak coupling with nitrogen.

To confirm this hypothesis, we performed 2D-HYSCORE experiments, which consist in transferring the electron magnetization to nuclear spin of surrounding nuclei in the structure. The results displayed in Figure 12, shows that in the (-,+) quadrant (strong coupling regime i.e. isotropic coupling constant $A_{iso} > 2\nu_i$, ν_i standing for the frequency of a given nuclei), we can observe a pattern arising from ^{14}N coupling with the observation of single quantum (sq) and double quantum (dq) transitions with an isotropic coupling constant A_{iso} of 6.1 MHz (calculated at the sq cross peaks position, here at ≈ 3.05 MHz). Additionally in the (+,+) quadrant (weak coupling regime i.e. $A_{iso} < 2\nu_i$) we can observed an anti-diagonal cross peak centered at 3.6 MHz and coming from Nb coupling with a maximum coupling of 4.1 MHz.

Complexes **1** and **3** exhibit the same HYSCORE pattern whereas for complex **2**, ^1H nuclear frequency (at 14.5 MHz, figure 12-middle) is observed coming from ^1H of pyridine molecules. Oxygen is not present due to its low physical occurrence, due to its measured ^{17}O isotope. The nuclei coupling pattern observed at X band was confirmed also at Q-band by recording 2D HYSCORE spectra for oxygen transition and Nb(IV) ones (Fig. S5b). For the Q-band experiment; we increase the frequency up to 34 GHz (instead of 9 GHz for X-band) resulting in the splitting of the different transitions, and were able to separate the oxygen component from the niobium(IV) ones. Same experiments also were conducted for complex **4**, but, the EPR experiment did not surprisingly give any signal. That led us to assume that the exchange of the electron between the *d* orbital of niobium and the *p* orbital of oxygen happens so quickly that cannot be detected in the frequencies of EPR. It would seem that the electron is more localized in the *p* orbital of oxygen than the *d* of niobium.

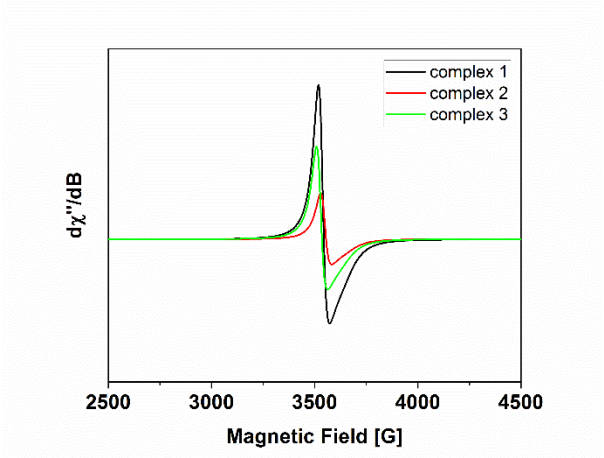

Figure 10. CW-EPR spectra of compounds **1** (black line), **2** (red line) and **3** (green line) recorded at room temperature.

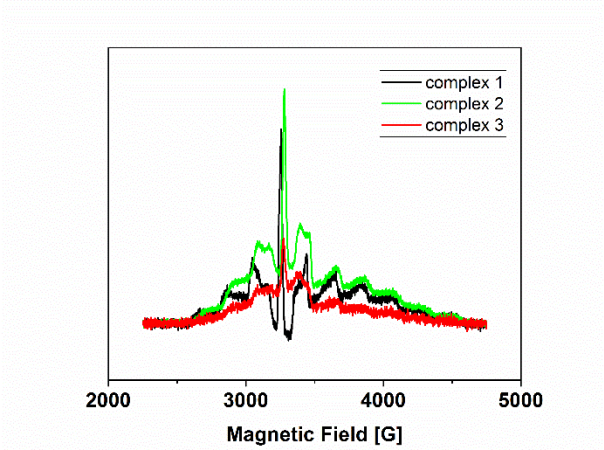

Figure 11. Echo field sweep experiments for compounds **1** (black line), **2** (red line) and **3** (green line).

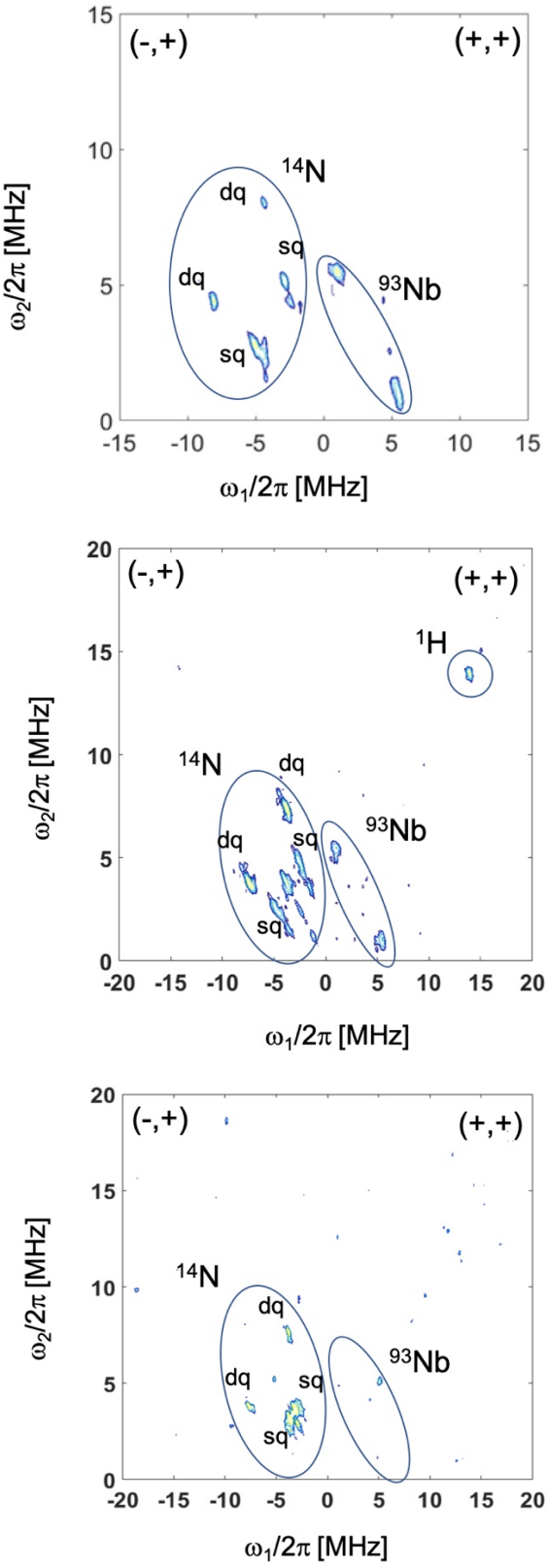

Figure 12. 2D-HYSCORE EPR experiments for compounds **1** (top), **2** (middle) and **3** (bottom), recorded at 5K.

X-Ray Photoelectron Spectroscopy (XPS)

Due to the unexpected absence of EPR signal related to the niobium(IV) oxidation state in complex **4**, we carried out an XPS analysis in order to further investigate its Nb *4d* electron configuration. We thus compared the XPS spectrum of compound **4**, with that of compound **1** (for which a EPR signature was typically observed due to Nb d^1 state, $g = 1.97$), and with that of Nb_2O_5, as a reference for niobium(V). The Figure 13 displays the Nb 3d spectra for the complexes **1, 4** and the Nb_2O_5 reference.

The Nb_2O_5 spectrum is characteristic for Nb(V) species, with a doublet peak corresponding to Nb $3d_{5/2}$ and Nb $3d_{3/2}$ with the binding energy (BE) values of 207.2 eV and 209.9 eV, respectively (energy splitting of 2.72 eV).[43] Complex **1** spectrum is composed of a doublet peak, shifted towards lower BE values as compared to Nb_2O_5 reference. The Nb $3d_{5/2}$ peak is localized at 206.4 eV and the spin-orbit splitting is 2.72 eV, which is characteristic of tetravalent state of Nb(IV) species.[44,45] This result is consistent with all the above characterization techniques (magnetism, EPR).

Regarding the Nb 3d spectrum for the complex **4**, it is as well composed of a doublet peak with the Nb $3d_{5/2}$ component localized at 206.4 eV and a spin-orbit splitting of 2.72 eV, which matches with the values observed for the complex **1**. We can thus confirm that complex **4** consists of Nb(IV) centers, so we can confirm that we have a series of Nb(IV) complexes.

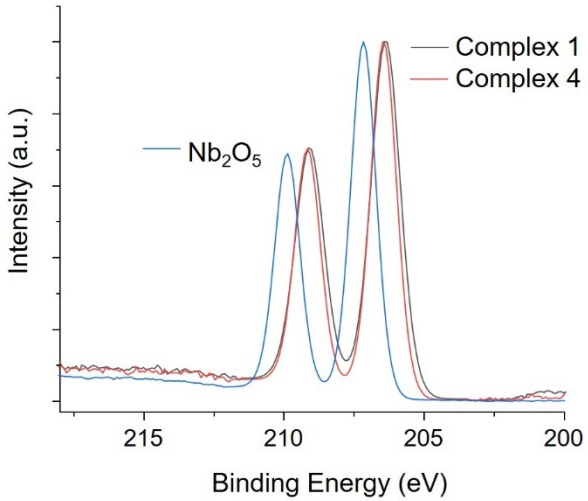

Figure 13. Room temperature XPS Nb 3d core level spectra of the complex **1** (red line), complex **4** (black line) and Nb_2O_5 (blue line).

Conclusion

This paper dealt with the synthesis and single-crystal X-ray diffraction analysis of four molecular coordination niobium(IV) complexes **1-4** utilizing either monoprotonated 2,3-pyridinedicarboxylate or 2,5-pyridinedicarboxylate as organic complexing ligands. The tetravalent oxidation state of this transition metal has been further characterized by magnetism measurements, EPR and XPS, which confirm the d^1 electronic configuration. However, no EPR signal was observed for complex **4**, which could be due to very rapid exchange of the electron between the *d* orbital of niobium and the *p* orbital of oxygen. All the niobium(IV) centers exhibit a similar coordination geometry, showing an eight-fold dodecahedral environment, with a $[Nb^{IV}O_4N_4]$ configuration, with four oxygen atoms from the monodentate carboxylate group and four neighboring nitrogen atoms from the pyridine fragment. This specific structural octa-

coordination geometry around the niobium(IV) follows the Orgel concept[37], previously reported in the niobium(IV) picolinate (2-pyridinecarboxylate).[29] Such a dodecahedral environment is thus expected for d^1 or d^2 transition metals, with mixed coordinated ligands such as carboxylato and pyridinato groups, which are considered as non-π-bonding (or π -donor) and π-bonding (or π -acceptor) ligands, respectively. This Nb-O and Nb-N interatomic bond lengths are characterized by shorter (2.084(3)-2.1084(11) Å) and longer (2.266(4)-2.296(4) Å) distances, respectively. Indeed, this stereochemistry around the niobium(IV) atom is observed to be stabilized by this mixed N,O attached ligands, remaining free the second carboxylic acid arm of pyridine ring, whatever its position (either in ortho or para position). Despite the addition of organic base with the aim to favor the deprotonation of the carboxylic acid function, our efforts to get promote a second linkage with the niobium(IV) centers through the second carboxylate group have failed. Future works will be focused on the use of polytopic organic spacers incorporating both N-acceptor and O-donor groups, in order to tentatively develop the multidimensional coordination polymer networks.

Notes

The authors declare no competing financial interest.

Acknowledgements

The authors would like to thank Mrs. Nora Djelal, Laurence Burylo, Céline Delabre and Philippe Devaux for their assistances with the synthesis, SEM images, XRD powder patterns measurements and chemical elementary analyses (UCCS). The "Fonds Européen de Développement Régional (FEDER)", "CNRS", "Région Hauts de France" and "Ministère de l'Education Nationale de l'Enseignement Supérieur et de la Recherche" are acknowledged for the funding of X-ray diffractometers from the Chevreul Institute platform.

Associated Content

Supporting Information

The Supporting Information is available free of charge at https://pubs.acs.org/doid/10.1021/acs.inorgchem.???

Optical and SEM photographs, powder XRD patterns, IR spectra; magnetic curves, EPR spectra.

Accession Codes

Crystallographic data for the structural analysis has been deposited with the Cambridge Crystallographic Data Centre, CCDC numbers 2171872 for **1**, 2171873 for **2**, 2171874 for **3** and 2171875 for **4**. Copies of the data can be obtained free of charge on application to CCDC, 12 Union Road, Cambridge CB2 1EZ (fax: +44-1223-336-033; e-mail: data_request@ccdc.cam.ac.uk).

References

(1) Cavka, J. H.; Jakobsen, S.; Olsbye, U.; Guillou, N.; Lamberti, C.; Bordiga, S.; Lillerud, K. P. A New Zirconium Inorganic Building Brick Forming Metal Organic Frameworks with Exceptional Stability. *J. Am. Chem. Soc.* **2008**, *130* (42), 13850–13851. https://doi.org/10.1021/JA8057953/SUPPL_FILE/JA8057953_SI_001.PDF.

(2) Winarta, J.; Shan, B.; McIntyre, S. M.; Ye, L.; Wang, C.; Liu, J.; Mu, B. A Decade of UiO-66 Research: A Historic Review of Dynamic Structure, Synthesis Mechanisms, and Characterization Techniques of an Archetypal Metal–Organic Framework. *Cryst. Growth Des.* **2019**, *20* (2), 1347–1362. https://doi.org/10.1021/ACS.CGD.9B00955.

(3) Hu, Z.; Wang, Y.; Zhao, D. The Chemistry and Applications of Hafnium and Cerium(Iv) Metal–Organic Frameworks. *Chem. Soc. Rev.* **2021**, *50* (7), 4629–4683. https://doi.org/10.1039/D0CS00920B.

(4) Jakobsen, S.; Gianolio, D.; Wragg, D. S.; Nilsen, M. H.; Emerich, H.; Bordiga, S.; Lamberti, C.; Olsbye, U.; Tilset, M.; Lillerud, K. P. Structural Determination of a Highly Stable Metal-Organic Framework with Possible Application to Interim Radioactive Waste Scavenging: Hf-UiO-66. *Phys. Rev. B - Condens. Matter Mater. Phys.* **2012**, *86* (12), 125429. https://doi.org/10.1103/PHYSREVB.86.125429/FIGURES/8/MEDIUM.

(5) Dan-Hardi, M.; Serre, C.; Frot, T.; Rozes, L.; Maurin, G.; Sanchez, C.; Férey, G. A New Photoactive Crystalline Highly Porous Titanium(IV) Dicarboxylate. *J. Am. Chem. Soc.* **2009**, *131* (31), 10857–10859. https://doi.org/10.1021/JA903726M/SUPPL_FILE/JA903726M_SI_002.CIF.

(6) Barthelet, K.; Marrot, J.; Riou, D.; Ferey, G. A Breathing Hybrid Organic ± Inorganic Solid with Very Large Pores and High Magnetic Characteristics. *Angew. Chem. Int. Ed* **2002**, *41* (2). https://doi.org/10.1002/1521-3773.

(7) Lammert, M.; Wharmby, M. T.; Smolders, S.; Bueken, B.; Lieb, A.; Lomachenko, K. A.; De Vos, D.; Stock, N. Cerium-Based Metal Organic Frameworks with UiO-66 Architecture: Synthesis, Properties and Redox Catalytic Activity. *Chem. Commun.* **2015**, *51* (63), 12578–12581. https://doi.org/10.1039/C5CC02606G.

(8) Loiseau, T.; Mihalcea, I.; Henry, N.; Volkringer, C. The Crystal Chemistry of Uranium Carboxylates. *Coord. Chem. Rev.* **2014**, *266–267* (1), 69–109. https://doi.org/10.1016/J.CCR.2013.08.038.

(9) Lv, K.; Fichter, S.; Gu, M.; März, J.; Schmidt, M. An Updated Status and Trends in Actinide Metal-Organic Frameworks (An-MOFs): From Synthesis to Application. *Coord. Chem. Rev.* **2021**, *446*, 214011. https://doi.org/10.1016/J.CCR.2021.214011.

(10) Griffin, S. L.; Champness, N. R. A Periodic Table of Metal-Organic Frameworks. *Coord. Chem. Rev.* **2020**, *414*, 213295. https://doi.org/10.1016/J.CCR.2020.213295.

(11) Ahn, S.; Thornburg, N. E.; Li, Z.; Wang, T. C.; Gallington, L. C.; Chapman, K. W.; Notestein, J. M.; Hupp, J. T.; Farha, O. K. Stable Metal−Organic Framework-Supported Niobium Catalysts. **2016**. https://doi.org/10.1021/acs.inorgchem.6b02103.

(12) Syzgantseva, M. A.; Ireland, C. P.; Ebrahim, F. M.; Smit, B.; Syzgantseva, O. A. Metal Substitution as the Method of Modifying Electronic Structure of Metal–Organic Frameworks. *J. Am. Chem. Soc.* **2019**, *141* (15), 6271–6278. https://doi.org/10.1021/JACS.8B13667.

(13) Korzyński, M. D.; Braglia, L.; Borfecchia, E.; Lomachenko, K. A.; Baldansuren, A.; Hendon, C. H.; Lamberti, C.; Dincă, M. Quo Vadis Niobium ? Divergent Coordination Behavior of Early-Transition Metals towards MOF-5. *Chem. Sci.* **2019**, *10* (23), 5906–5910. https://doi.org/10.1039/C9SC01553A.

(14) Rivera-Torrente, M.; Hernández Mejía, C.; Hartman, T.; de Jong, K. P.; Weckhuysen, B. M. Impact of Niobium in the Metal–Organic Framework-Mediated Synthesis of Co-

Based Catalysts for Synthesis Gas Conversion. *Catal. Letters* **2019**, *149* (12), 3279–3286. https://doi.org/10.1007/S10562-019-02899-0/TABLES/1.
(15) Cadiau, A.; Adil, K.; Bhatt, P. M.; Belmabkhout, Y.; Eddaoudi, M. A Metal-Organic Framework–Based Splitter for Separating Propylene from Propane. *Science (80-.).* **2016**, *353* (6295), 137–140. https://doi.org/10.1126/SCIENCE.AAF6323.
(16) Mileo, P. G. M.; Adil, K.; Davis, L.; Cadiau, A.; Belmabkhout, Y.; Aggarwal, H.; Maurin, G.; Eddaoudi, M.; Devautour-Vinot, S. Achieving Superprotonic Conduction with a 2D Fluorinated Metal-Organic Framework. *J. Am. Chem. Soc.* **2018**, *140* (41), 13156–13160. https://doi.org/10.1021/JACS.8B06582/SUPPL_FILE/JA8B06582_SI_001.PDF.
(17) Bhatt, P. M.; Belmabkhout, Y.; Cadiau, A.; Adil, K.; Shekhah, O.; Shkurenko, A.; Barbour, L. J.; Eddaoudi, M. A Fine-Tuned Fluorinated MOF Addresses the Needs for Trace CO2 Removal and Air Capture Using Physisorption. *J. Am. Chem. Soc.* **2016**, *138* (29), 9301–9307. https://doi.org/10.1021/JACS.6B05345/SUPPL_FILE/JA6B05345_SI_003.CIF.
(18) Tchalala, M. R.; Belmabkhout, Y.; Adil, K.; Chappanda, K. N.; Cadiau, A.; Bhatt, P. M.; Salama, K. N.; Eddaoudi, M. Concurrent Sensing of CO 2 and H 2 O from Air Using Ultramicroporous Fluorinated Metal-Organic Frameworks: Effect of Transduction Mechanism on the Sensing Performance. *ACS Appl. Mater. Interfaces* **2019**, *11* (1), 1706–1712. https://doi.org/10.1021/ACSAMI.8B18327/SUPPL_FILE/AM8B18327_SI_001.PDF.
(19) Tchalala, M. R.; Bhatt, P. M.; Chappanda, K. N.; Tavares, S. R.; Adil, K.; Belmabkhout, Y.; Shkurenko, A.; Cadiau, A.; Heymans, N.; De Weireld, G.; Maurin, G.; Salama, K. N.; Eddaoudi, M. Fluorinated MOF Platform for Selective Removal and Sensing of SO2 from Flue Gas and Air. *Nat. Commun. 2019 101* **2019**, *10* (1), 1–10. https://doi.org/10.1038/s41467-019-09157-2.
(20) Yang, L.; Cui, X.; Zhang, Z.; Yang, Q.; Bao, Z.; Ren, Q.; Xing, H. An Asymmetric Anion-Pillared Metal–Organic Framework as a Multisite Adsorbent Enables Simultaneous Removal of Propyne and Propadiene from Propylene. *Angew. Chemie* **2018**, *130* (40), 13329–13333. https://doi.org/10.1002/ANGE.201807652.
(21) Ziebel, M. E.; Ondry, J. C.; Long, J. R. Two-Dimensional, Conductive Niobium and Molybdenum Metal-Organic Frameworks †. **2020**. https://doi.org/10.1039/d0sc02515a.
(22) Chen, X.; Peng, X.; Jiang, L.; Yuan, X.; Yu, H.; Wang, H.; Zhang, J.; Xia, Q. Recent Advances in Titanium Metal–Organic Frameworks and Their Derived Materials: Features, Fabrication, and Photocatalytic Applications. *Chem. Eng. J.* **2020**, *395*, 125080. https://doi.org/10.1016/J.CEJ.2020.125080.
(23) Wang, S.; Reinsch, H.; Heymans, N.; Wahiduzzaman, M.; Martineau-Corcos, C.; De Weireld, G.; Maurin, G.; Serre, C. Toward a Rational Design of Titanium Metal-Organic Frameworks. *Matter* **2020**, *2* (2), 440–450. https://doi.org/10.1016/J.MATT.2019.11.002.
(24) Nguyen, H. L. The Chemistry of Titanium-Based Metal–Organic Frameworks. *New J. Chem.* **2017**, *41* (23), 14030–14043. https://doi.org/10.1039/C7NJ03153J.
(25) Andriotou, D.; Duval, S.; Volkringer, C.; Trivelli, X.; Shepard, W.; Loiseau, T. Structural Variety of Niobium(V) Polyoxo Clusters Obtained from the Reaction with Aromatic Monocarboxylic Acids: Isolation of {Nb2O}, {Nb4O4} and {Nb8O12} Cores. *Chem. - A Eur. J.* **2022**, *submitted*.
(26) Cotton, A.; Diebold, M. P.; Roth, W. J. Dinuclear Niobium (IV) Complexes Nb2Cl4 (OMe) 4L2 (L Relation to Analogous W and Mo Compounds. **1987**, *4* (Iv), 3319–3322. https://doi.org/10.1021/ic00267a021.
(27) Arimondo, P. B.; Calderazzo, F.; Englert, U.; Maichle-Mössmer, C.; Pampaloni, G.;

Strähle, J. Preparation and Characterization of Dialkylcarbamato Derivatives of Niobium and Tantalum. *J. Chem. Soc. Dalt. Trans.* **1996**, No. 3, 311–319. https://doi.org/10.1039/DT9960000311.
(28) Calderazzo, F.; Englert, U.; Maichle-Mössmer, C.; Marchetti, F.; Pampaloni, G.; Petroni, D.; Pinzino, C.; Strähle, J.; Tripepi, G. Eight-Coordinate Chelate Complexes of Zirconium(IV) and Niobium(IV): X-Ray Diffractometric and EPR Investigations. *Inorganica Chim. Acta* **1998**, *270* (1–2), 177–188. https://doi.org/10.1016/S0020-1693(97)05838-6.
(29) Ooi, B. L.; Sakane, G.; Shibahara, T. Synthesis and Crystal Structure of Tetrakis(2-Pyridinecarboxylato)Niobium(IV)-2-Ethanol, an Octacoordinate Dodecahedral D1 M(A-B)4 System. *Inorg. Chem.* **1996**, *35* (25), 7452–7454. https://doi.org/10.1021/IC960803G/SUPPL_FILE/IC7452.PDF.
(30) Kirby1, R.; Freiser, H. Polarography of Niobium-EDTA Complexes. **2022**, *10*, 13.
(31) Ooi, B. L.; Xu, Q.; Shibahara, T. Structural Characterization of an Eight-Coordinate Nb(IV)-Edta Complex, [Nb(Edta)(H2O)2]·2H2O. *Inorganica Chim. Acta* **1998**, *274* (1), 103–107. https://doi.org/10.1016/S0020-1693(97)05900-8.
(32) Ooi, B. L.; Søtofte, I.; Vittal, J. J. Synthesis and Structure of Cyclic Hexanuclear Oxo-Alkoxo–Carboxylatoniobium(IV) Complexes. *Inorganica Chim. Acta* **2004**, *357* (2), 625–629. https://doi.org/10.1016/J.ICA.2003.08.016.
(33) SAINT, Version 8.34A, Bruker AXS Inc., Madison, Wisconsin, USA, 2014.
(34) Krause, L.; Herbst-Irmer, R.; Sheldrick, G. M.; Stalke, D. Comparison of Silver and Molybdenum Microfocus X-Ray Sources for Single-Crystal Structure Determination. *J. Appl. Crystallogr.* **2015**, *48* (1), 3–10. https://doi.org/10.1107/S1600576714022985/AJ5242SUP14.PDF.
(35) Sheldrick, G. M. Crystal Structure Refinement with SHELXL. https://doi.org/10.1107/S2053229614024218.
(36) Dolomanov, O. V.; Bourhis, L. J.; Gildea, R. J.; Howard, J. A. K.; Puschmann, H. OLEX2: A Complete Structure Solution, Refinement and Analysis Program. *urn:issn:0021-8898* **2009**, *42* (2), 339–341. https://doi.org/10.1107/S0021889808042726.
(37) Orgel, L. E. The [Mo(CN)8]4− Structure. *J. Inorg. Nucl. Chem.* **1960**, *14* (1–2), 136–138. https://doi.org/10.1016/0022-1902(60)80215-1.
(38) Peterson, E. J.; Von Oreele, R. B.; Brown, T. M. Crystal and Molecular Structure of Tetraisothiocyanatobis(2,2′-Bipyridine)Niobium(IV) and -Zirconium(IV). *Inorg. Chem.* **1976**, *15* (2), 309–315. https://doi.org/10.1021/IC50156A014/SUPPL_FILE/IC50156A014_SI_001.PDF.
(39) Lippard, S. J.; Russ, B. J. Comment on the Choice of an Eight-Coordinate Polyhedron. *Inorg. Chem.* **1968**, *7* (8), 1686–1688. https://doi.org/10.1021/IC50066A058.
(40) P.W. Selwood Magnetochemistry (2nd ed.), Interscience Publishers, New York (1956).
(41) Deutscher, R. L.; Kepert, D. L. Eight Coordinate Tetrakis-Chelate Complexes of Niobium(IV) and Tantalum(IV). *Inorganica Chim. Acta* **1970**, *4* (C), 645–650. https://doi.org/10.1016/S0020-1693(00)93370-X.
(42) Steunou, N.; Bonhomme, C.; Sanchez, C.; Vaissermann, J.; Hubert-Pfalzgraf, L. G. A Tetranuclear Niobium Oxo Acetate Complex. Synthesis, X-Ray Crystal Structure, and Characterization by Solid-State and Liquid-State NMR Spectroscopy. *Inorg. Chem.* **1998**, *37* (5), 901–910. https://doi.org/10.1021/ic971024i.
(43) Özer, N.; Chen, D. G.; Lampert, C. M. Preparation and Properties of Spin-Coated Nb2O5 Films by the Sol-Gel Process for Electrochromic Applications. *Thin Solid Films* **1996**, *277* (1–2), 162–168. https://doi.org/10.1016/0040-6090(95)08011-2.
(44) Fontaine, R.; Caillat, R.; Feve, L.; Guittet, M. J. Déplacement Chimique ESCA Dans

La Série Des Oxydes Du Niobium. *J. Electron Spectros. Relat. Phenomena* **1977**, *10* (4), 349–357. https://doi.org/10.1016/0368-2048(77)85032-9.
(45) Weibin, Z.; Weidong, W.; Xueming, W.; Xinlu, C.; Dawei, Y.; Changle, S.; Liping, P.; Yuying, W.; Li, B. The Investigation of NbO2 and Nb2O5 Electronic Structure by XPS, UPS and First Principles Methods. *Surf. Interface Anal.* **2013**, *45* (8), 1206–1210. https://doi.org/10.1002/SIA.5253.